Applied Physics A (2020) 126:696
https://doi.org/10.1007/s00339-020-03890-y

Applied Physics A
Materials Science & Processing

Raman, FTIR studies and optical absorption of zinc borate glasses containing WO_3

M. Farouk[1] · A. Samir[2] · A. Ibrahim[3] · M. A. Farag[1] · A. Solieman[4]

Received: 10 June 2020 / Accepted: 5 August 2020

Abstract
Glasses with composition [$x$$WO_3$–(25−$x$)–ZnO–20$Na_2O$–55$B_2O_3$ where x = 0, 5, 10, 15 and 20 mol. %] were prepared by melt quenching method. The amorphous state of the current glass samples was checked by X-ray diffraction (XRD). The measured density and calculated molar volume of all prepared samples were found to increase with the replacement of the lighter ZnO by the heavier of WO_3. The network structure of the present glasses was studied using the infrared (IR) and Raman spectroscopic techniques. IR and Raman results show that the structure of the samples is BO_3 and BO_4 units located in several structural groups with W–O–W units. The decreasing of the band gap energy values by the introducing of WO_3 showed that the creation increases of the number of non-bridging oxygens in the structure of glass. All results showed that the parameters were dependent upon the dopant concentration of WO_3 in the prepared glasses.

Keywords Infrared · Raman · Optical · Structure · WO_3 · Borate glass

1 Introduction

Glass systems containing tungsten ions have a great interest because of their unique thermal, electrical and optical properties such as photochromism for important applications, which are known for a color change because of the movement of electromagnetic radiation [1–10]. Because of this reason, the type of this glass is useful for applications in photonic devices of a large memory, smart windows to control solar input of semiconductor houses [11, 12]. These properties depend on the existence of tungsten in several valance states such as W^{6+}, W^{5+} and W^{4+} [12, 13].

The tungsten W^{6+} ions take part in the glass network with various structural groups as WO_4 tetrahedral and WO_6 octahedral. On the other hand, W^{5+} ions ($5d^1$ are known paramagnetic ions) participate in the shape of $W^{5+}O_3^-$ and occupy octahedral (O_h) positions [12, 14, 15]. Therefore, the existence of tungsten ions in many oxidation states and structural units in the glass system at a given temperature depends on the modifiers, formers, mobility of the modifier cation [12, 16–18]. Borate glass exhibit importance materials for engineering technology because of their low melting point (T_m), high transparency, thermal stability, good glass former, easy to process, nontoxic, high density, shielding for IR radiations and used to make dielectric materials [19–22]. The addition of alkali oxides to borate glasses reduces the melting point (T_m), enhance the physical properties of these glasses like their preparation conditions [23].

Alkali borate glasses are important substances in electro-optic, optical fibers due to its technological side, and in nonlinear devices for frequency conversion in the UV range and piezoelectric actuator [24]. The two forms of boron coordination have been reported, $BO_3$and BO_4.In addition, the conversion of BO_3into BO_4 units is depending on the concentration, nature and type of the added modifiers [8, 25–27]. Raman scattering and infrared spectroscopy have shown to be powerful and active tools for describing the structure of ligand field in glasses [2, 28, 29]. ZnO enters the host of the glass in the form of network former or modifier. Therefore, ZnO acting as a network modifier is known to

✉ M. Farouk
m_farouk@azhar.ed.eg; mf_egypt22375@yahoo.com

[1] Physics Department, Faculty of Science, Al-Azhar University, Nasr City, Cairo 11884, Egypt

[2] Engineering Mathematics and Physics Department, Faculty of Engineering at Shoubra, Benha University, Cairo 11629, Egypt

[3] Basic Sciences Department, Faculty of Engineering Science, Sinai University, El Kantara, Egypt

[4] Physics Department, Faculty of Science, Al-Azhar University, Assuit branch, Cairo, Egypt

Published online: 12 August 2020

importantly modify different glass properties [6, 30–33]. On the other hand, the addition of ZnO to borate glasses reduces the melting properties due to the fact that it has a high polarizability [19]. The objective of the current work is to study the behavior and effect of replacement of ZnO by WO_3 on the structure of local arrangements and optical properties by Fourier Transform infrared (FTIR), Raman scattering and UV–Vis spectroscopy of alkali borate glasses and to obtain a bulk glass samples from these glass compositions that could be interesting for the optical, thermochromic, photochromic and electrocromic applications.

2 Experimental setup

The glass system with composition [xWO$_3$–(25 − x)–ZnO–20Na$_2$O–55B$_2$O$_3$ where x = 0, 5, 10, 15 and 20 mol.%] were prepared by melt quenching method using an appropriate mixture of chemicals H_3BO_3, Na_2CO_3, ZnO and WO_3. Each batch approximately 30 g of powder form was weighed using a digital balance with an accuracy of 10^{-4}. The mixed powder was completely melted in a porcelain crucible in an electric furnace at 1100 °C for about 30 min. The melt was continued sometimes to ensure homogeneity. The melt is then poured at room temperature onto a polished brass plate and quickly pressed to a thickness of ~ 1 mm by another brass plate. The amorphous nature of the prepared samples was checked by X-ray diffraction (XRD) spectrum on Philips- PW3720 at a scanning angle 2θ varied from 5 to 80. The density (ρ) of glass samples was measured by Archimedes method using carbon tetrachloride as buoyant fluid ($\rho = 1.592$ g/cm^3). The molar volume ($V_m = M_w/\rho$) of the samples was calculated using the relation $V_m = M_w/\rho$ where W_M is the total molecular weight. The measurements were repeated three times and the average value was used. FTIR absorption spectra of all samples were measured at room temperature using (FTIR Nicolet 6700) spectrometer in the range of 400–1600 cm^{-1} using KBr pellet technique. The structure of the glass samples was analysis at room temperature by Raman spectroscopy using confocal MR520 with green excitation laser of 532 nm. The Raman spectra were gained in a backscattering geometry between 200 and 1600 cm^{-1}. The optical absorption spectra of polished, prepared glasses are measured at room temperature using a JENWAY 6405 UV/Vis. Spectrophotometer in the wavelength range 190–1100 nm.

3 Results and discussion

The X-ray diffraction spectra of the prepared samples are shown in Fig. 1. The spectra show no diffraction peaks (sharp peaks), revealing the amorphous nature of the glass samples. The increase of the WO_3 content does not affect the amorphous state of the samples. This is confirming the forming of the glasses containing WO_3. This is in agreement with the previously published date for similar glass systems.

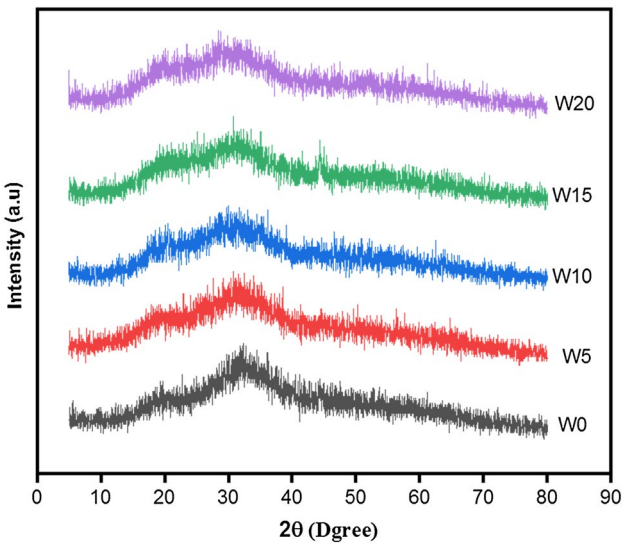

Fig. 1 X-ray diffraction patterns of the investigated samples

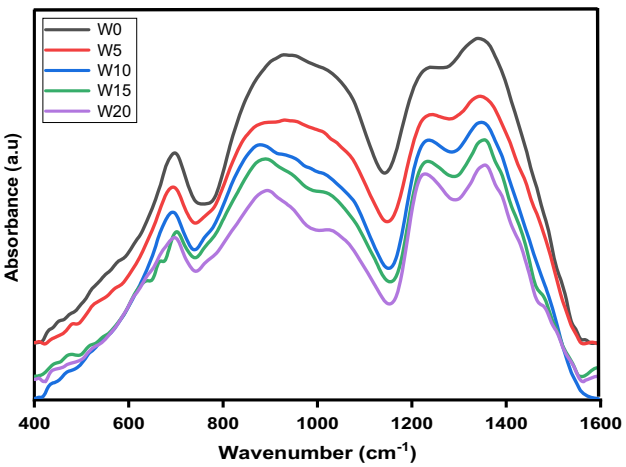

Fig. 2 IR spectra of the samples doped with different concentrations of WO_3

3.1 Infrared spectral studies

Figure 2 shows the IR spectra of the prepared glass samples in the range of 400–1600 Cm^{-1} as a function of WO_3 content. The structural units of the borate glasses, BO_3 and BO_4 are basically active in this range. The spectra mainly show three strong, broad absorption peaks varying in intensity by the change of the composition of the glass. Each infrared spectrum of the present study was deconvoluted using

10–11 Gaussian functions to characterize perfect the position of absorption peak and their intensity variation, shown in Fig. 3. The obtained absorption peak positions and their assignments are given in Table 1. The band at ~ 598 cm^{-1} can be assigned to the borate deformation such as the in-plane bending of BO_3 unit and shift to lower wave number with increasing of WO_3 content [34, 35]. The peak located around ~ 698 cm^{-1} is attributed to bending vibrations of pentaborate groups. The intensity of this peak decreases as a function of WO_3 content [10, 15, 35]. In addition, of WO_3 (at 5 mol. %), the weak new band appears at ~ 759 cm^{-1}can be assigned to B–O–B bending vibrations of BO_3, BO_4 groups with W–O–W vibrations and its intensity increase with the increasing of WO_3 concentration [10, 35–38]. This indicates that the tungsten enters as a network former. The absorption band at about ~ 856 cm^{-1} is due to stretching of BO_4 units [39, 40]. With increasing of WO_3 content, this band shifted to ~ 893 cm^{-1} and also assigned to starching vibration of non-bridging oxygens (NBOs) of BO_4 groups overlapping with the stretching vibrations of WO4 units [15, 35, 41]. IR band located at ~ 959–985 cm^{-1} is attributed to the stretching vibrations of B–O bonds in BO_4unit and overlapping with the WO_6 units [35, 42]. For the blank sample the band around ~ 1034 cm^{-1} is due to stretching vibrations of B–O bonds in BO_4 units from tri-, tetra- and penta- borate groups and this band shift to lower wave number with adding of WO_3 [43–45]. The band centered at ~ 1100 cm^{-1} is attributed to pentaborate units [35, 46]. B–O stretching vibrations ofBO_3 unit in meta-borate chains and orthoborate found at ~ 1204–1226 cm^{-1}, these bands can be characterized for the presence of a large number of non-bridging oxygen (NBO's) at high concentration of WO_3 (20 mol.%) [35, 41, 45]. This means that the conversion of the BO_4 of the BO_3 units containing NBOs and it is clear from a calculated of

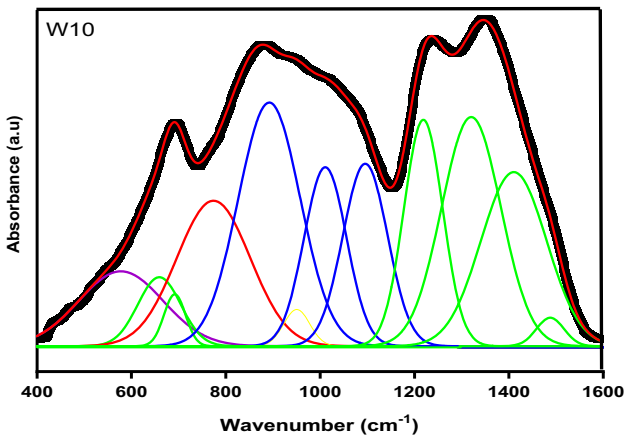

Fig. 3 Deconvoluted infrared bands of the samples doped with WO_3 = 10 mol.%

Table 1 Band assignments for IR spectra of the prepared samples

Band center (cm^{-1})					Band assignment
W0	W5	W10	W15	W20	
601	576	578	538	556	Assigned to the borate deformation such as the in-plane bending of BO_3 unit and shift to lower wave number with increasing of WO_3 content [34, 35]
621	647	660	645	648	
697	698	693	702	697	Attributed to bending vibrations of pentaborate groups. The intensity of this peak decreases as a function of WO_3 content [10, 15, 35]
–	757	775	764	776	Assigned to B-O-B bending vibrations of BO_3, BO_4 groups with W–O-W vibrations and its intensity increase with the increasing of WO_3 concentration [10, 35–38]
855	863	893	869	879	Is due to stretching of BO_4 units [39, 40]. With increasing of WO_3 content, this band shifted to ~ 893 cm^{-1} and also assigned to starching vibration of non-bridging oxygens (NBOs) of BO4 groups overlapping with the stretching vibrations of WO4 units [15, 35, 41]
960	–	952	955	964	Attributed to the stretching vibrations of B-O bonds in BO_4 unit and overlapping with the WO_6 units [35, 42]
1034	1011	1012	–	–	Is due to stretching vibrations of B-O bonds in BO_4 units from tri, tetra and penta borate groups and this band shift to lower wave number with adding of WO_3 [43–45]
1097	1099	1097	1067	1078	Is attributed to penta borate units [35, 46]
1204	1224	1221	1229	1226	B-O stretching vibrations of BO_3 unit in meta-borate chains and orthoborate found at ~ 1204–1226 cm^{-1}, these bands can be characterized for the presence of a large number of non-bridging oxygen (NBO's) at high concentration of WO_3 (20 mol%) [35, 41, 45]
1274	–	–	–	–	Asymmetric stretching vibrations of the B-O of BO_3 units of meta, pyro and orthoborate units [34, 35, 42]
–	1342	1322	1343	1340	
1379	–	–	–	1371	
–	–	1413	1437	1438	
1477	1493	1490	1502	1496	The strong band at ~ 1484 cm^{-1} can be attributed to the B-O bond asymmetric stretching in the BO_3 groups [47]

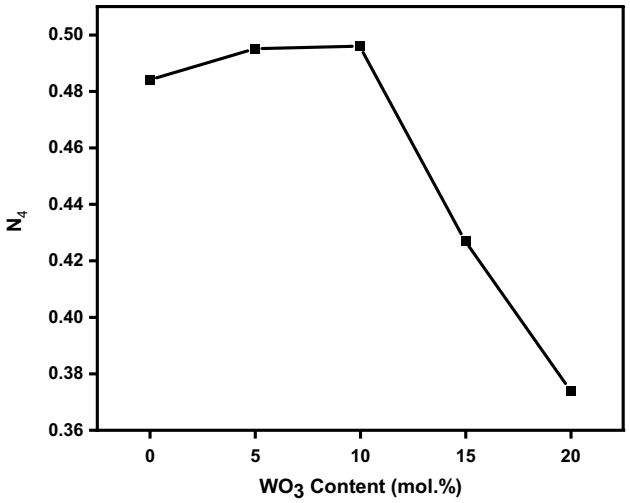

Fig. 4 The relation between N_4 and WO_3 content

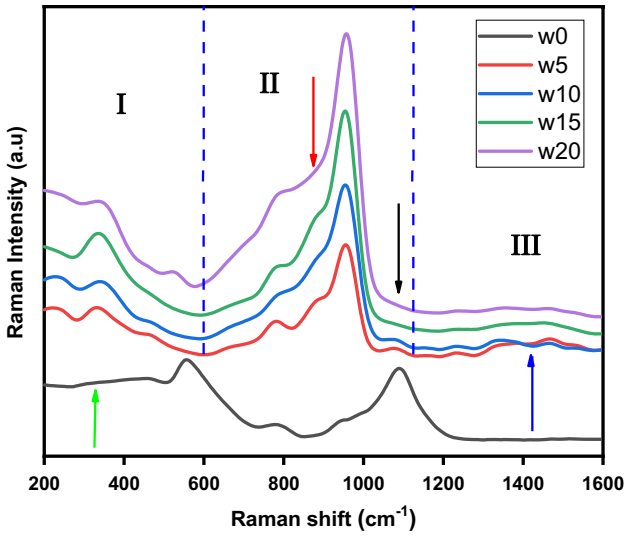

Fig. 5 Raman spectra of the glass samples with different concentrations WO_3

N_4 in Fig. 4. Asymmetric stretching vibrations of the B–O of BO_3units of meta, pyro and orthoborate units can exist at ~ 1380 cm^{-1} [34, 35, 42]. The strong band at ~ 1484 cm^{-1} can be attributed to the B–O bond asymmetric stretching in the BO_3 groups [47].

3.2 Raman studies

Raman spectroscopy is the technique used to characterize the molecular composition or vibrations and investigate the structure of a glass sample. The room temperature Raman spectra of the present samples are shown in Fig. 5. Each Raman spectrum was deconvoluted using Gaussian functions to obtain the position of the bands and their intensity, see Fig. 6. The Raman band positions of all the glass samples according to the literatures are listed in Table 2. There are three regions clearly in the Raman spectra (Fig. 5): (I) 200–600 cm^{-1}, (II) 600–1100 cm^{-1} and (III) 1100–1600 cm^{-1}. From the Raman spectra, it observed that each band represents either borate former or modifier ion. The broadening of Raman spectra due to the higher degree of disorders in the matrix of glass samples and also maybe the overlapping of more than one band. The first region (I) of Raman spectra at 200–600 cm^{-1} are attributed to different of groups of ZnO, alkali, B_2O_3 and WO_3. The vibrational modes of Zn–O bonds from ZnO_4 groups, bending modes of ZnO_4 units, containing both BO_3 triangles and BO_4 tetrahedral, vibrations of W–O–W bonds in WO_6 units and the symmetric bending modes in $(WO_4)^{2-}$ units [2, 4, 48]. In the second region (II) the vibrational bands at 856–901 cm^{-1} is due to stretching vibrations of W–O–W in the WO_4 or WO_6 units. The strong band centered at 960 cm^{-1} which is assigned to W–O– stretching vibrations in WO_4 tetrahedral and tends to shift toward higher Raman shift with increasing of WO_3 content and/or Stretching vibrations of W–O– and W=O bonds in WO_4 tetragonal or WO_6 octagonal units overlapping with stretching vibrations of B–O linkages in BO_4 tetrahedral, i.e. at this band can be ascribed to the incorporation of tungsten ions into the borate network and the formation of mixed structural units [48–51]. It is known that W^{6+} ions in glass systems can take the various states of WO_4 tetrahedron and WO_6 octahedron, depending on the glass composition [4]. While the band observed around 724–776 cm^{-1} which is a signed to a six-member ring with one or two BO_4 tetrahedral and shift towards higher wavenumber with increasing of WO_3 content [2]. Raman band in the range at 637–676 cm^{-1} attributed to the pent borate in the borate glass systems [2, 52].

Finally, in the third region (III), the Raman bands at 1333–1529 cm^{-1} are attributed to stretching of B–O_ in large numbers of borate rings, and stretching vibrations of B–O bonds involving NBOs [53–56]. The structural groups identified from the IR and Raman spectra, respectively it is reasonable to known of the network formers/modifiers like ZnO and WO_3 exists mainly in ZnO_4 structural units, WO_4 tetrahedral and WO_6 distorted octahedral structural units; B_2O_3 exists in BO_3 trigonal and BO_4 tetrahedral with NBOs structural units.

3.3 Density and molar volume parameters

Figure 7 shows the variation of molar volume and density as a function of WO_3 content. Normally, density and the molar volume have opposite behavior to each other; this is not fulfilled in the present system. However, this abnormal behavior was reported earlier for many glass systems [39, 50].

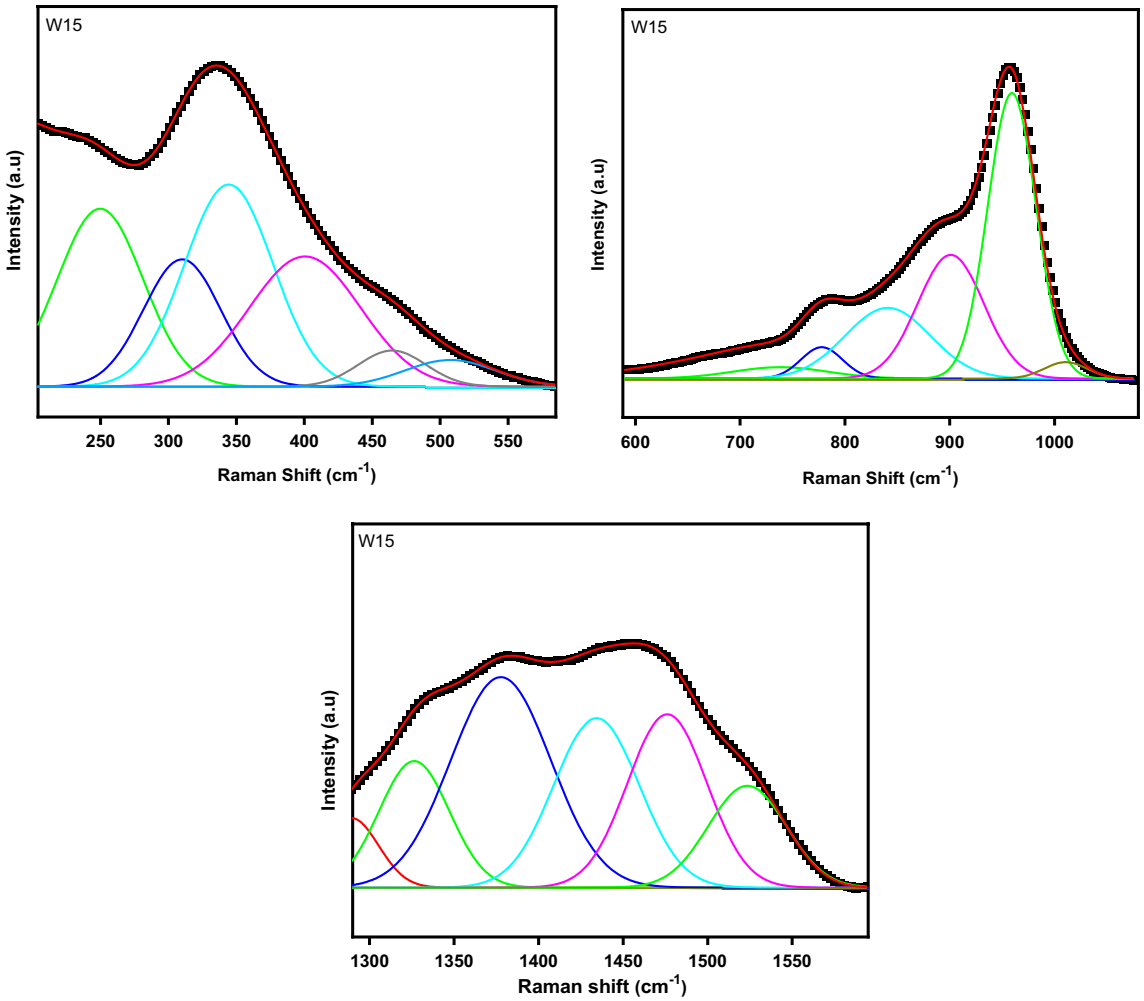

Fig. 6 Deconvoluted Raman bands of the samples doped with $WO_3 = 15$ mol%

Table 2 Identified Raman bands and their assignments for the prepared glasses

Sample code	Raman spectral band regions (cm^{-1})		
	Region I (200–600)	Region II (600–1100)	Region III (1100–1600)
W0	107–425–470–562	612–786–964–1045–1095–1145	–
W5	169–245–300–334–384–416–462–520–565	674–714–731–758–777–853–891–941–963–976	1317–1327–1378–1439–1480–1529–1574
W10	165–234–261–308–346–376–413–462–500	682–723–778–781–843–899–960	1305–1330–1374–1436–1474–1509–1534–1545
W15	178–250–310–344–401–465–508	712–738–778–841–901–960–1011	1289–1326–1377–1434–1476–1524–1530
W20	201–241–279–330–368–400–474–528	663–719–777–830–921–965–975–1046	1137–1240–1281–1328–1399–1477–1533–1554

The increase in the density of glass samples because of the exchange of the light weight of ZnO ($M_w = 81.38$ g/mol.) by the higher molecular weight of WO_3 ($M_w = 231.84$ g/mol.) in the glass composition, which are the major structures in the present glass. For this reason, the denser amorphous structures are carried out due to stronger cross-linking between borate networks. Moreover, the increase in the density of glass samples is due to the formation of WO_4 or WO_6 structural units of tungsten ions in the glass matrix [10]. The formation of non-bridging oxygen (convert of BO_4 to BO_3)

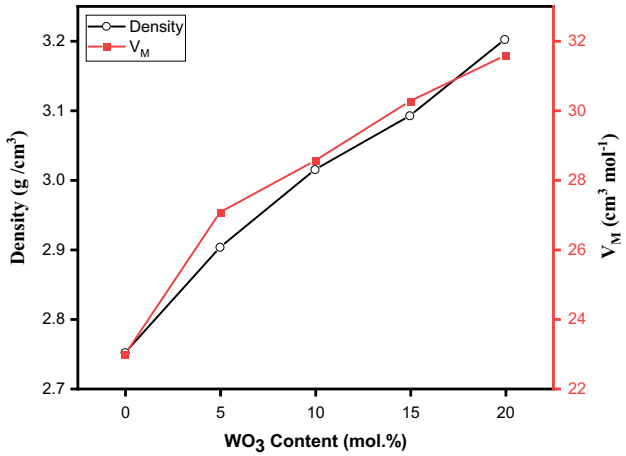

Fig. 7 Variation of the density and molar volume with WO_3 content

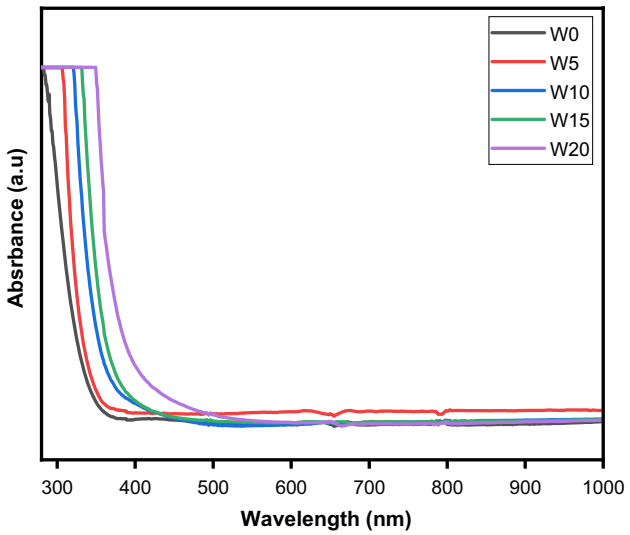

Fig. 8 Optical absorption spectra of the prepared glass

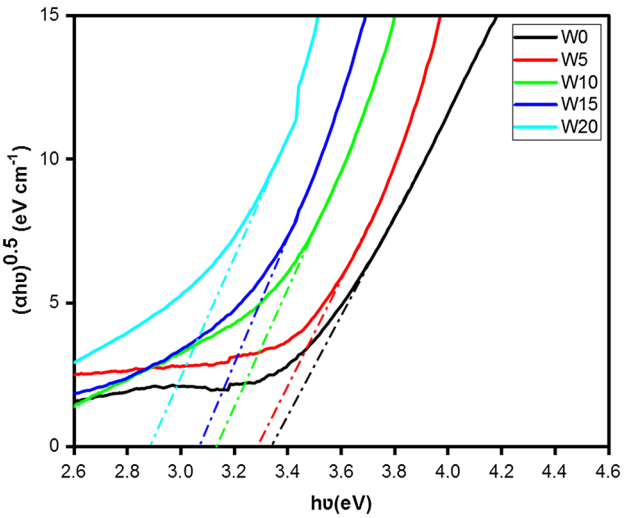

Fig. 9 $(\alpha h\upsilon)^{0.5}$ as a function of photon energy of the synthesized samples

Table 3 The density, molar volume, optical band gap (E_{opt}), Urbach energy (ΔE) and refractive index (n_r) for the samples

Sample code	ρ (g/cm^3)	V_M (cm^3/mol)	Optical parameters		
			E_{opt} (eV)	ΔE (eV)	n_r
W0	2.750	22.967	3.34	0.2064	1.529
W5	2.902	27.058	3.29	0.2172	1.546
W10	3.014	28.547	3.13	0.2274	1.559
W15	3.092	30.263	3.06	0.2371	1.568
W20	3.202	31.573	2.89	0.2808	1.581

may be related to the expansion of the glass structure causing an increase in the molar volume of present glass samples, see in IR results as described above. On the other hand, the increase of molar volume in tungsten glasses means that the rises gradually of oxygen induces the formation of NBOs with increasing of WO_3 content [57]. Therefore, the addition of WO_3 can boost a relatively open structure causing an increase in the molar volume [50].

3.4 Optical absorption

The optical absorption spectra of polished glass samples were recorded at room temperature and are shown in Fig. 8. The prepared glasses appear transparent to the naked eye with a slightly yellowish color increase when tungsten increases. Therefore, the valance of W ions exists in both forms W^{6+} and W^{5+} ions in glasses [4]. Figure 8 shows no absorption peaks exhibited for all glass samples in this range. The UV–Vis absorption edges of the prepared glasses are not sharply defined which indicating the amorphous nature of glass samples. The absorption edge of the glass samples is found to be shifted gradually towards longer wavelengths (red shift) with an increase of the WO_3content.This shift can be due to the increase in the NBOs, which in turn gives a boost to a decrease in bridging oxygen [12]. The energy band gap (E_{opt}) can be determined by plots drawn between $(\alpha h\nu)^{1/2}$ and hν as shown in Fig. 9 [58]. The determined values of the band gap (E_{opt}) energy for indirect transition are given in Table 3. The variation of E_{opt} may be assigned to the network structural changes. Therefore, the increase in the NBOs decreases the band gap energy as a function of WO_3 [10, 50, 59]. This result agreed with infrared and Raman data of the present glass samples above. Band tails energy (ΔE) which reveals the information about the density of localized states in the band gap, which is obtained from the plots between $h\nu$ versus ln$\alpha(\nu)$ (not shown) [60]. The

values of ΔE are calculated by taking the reciprocals of the slopes of the linear part of the ln$\alpha(\nu)$ versus $h\nu$ plots. Thus, the values of band tail energy of the prepared samples are listed in Table 3. From the table, the values of ΔE increases with increasing of the WO_3 content which indicates that the number of localized states inside the band gap increases.

4 Conclusions

The current glass system was prepared, and their structural and optical properties were studied using IR, Raman and UV–Vis spectroscopy. IR and Raman results exhibit many bands characteristic of borate network and tungsten structural units. It was found that the addition of WO_3 into these prepared glasses increase the formation of NBOs. The values of E_{opt} decrease with increasing of WO_3 content, this due to the increases of NBOs content. In addition, both E_{opt} and the ΔE are opposite trend.

References

1. K.S. Rao, V.R. Kumar, N. Veeraiah, Mater. Chem. Phys. **111**, 283–292 (2008)
2. A. Edukondalu, A. Hameed, B. Kavitha, R.V. Kumar, K.S. Kumar, Mater. Today. Process **2**, 913–917 (2015)
3. D. Deal, M. Burd, R. Braunstein, J. Non-Cryst, Solids **54**, 207 (1983)
4. Y. Taki, K. Shinozaki, T. Honma, V. Dimitrov, T. Komatsu, J. Solid State Chem. **220**, 191–197 (2014)
5. M. Ataalla, A.S. Afify, M. Hassan, M. Abdallah, M. Milanova, H.Y. Aboul-Enein, A. Mohamed, J. Non Cryst. Solids **491**, 43–54 (2018)
6. Y. Gandhi, I.V. Kityk, M.G. Brik, P.R. Rao, N. Veeraiah, J. Alloy. Compd. **508**, 278–291 (2010)
7. G. Pal Singh, P. Kaur, S. Kaur, D.P. Singh, Phys. B **406**, 4652–4656 (2011)
8. A. Edukondalu, B. Kavitha, M.A. Samee, S.K. Ahmmed, S. Rahman, K.S. Kumar, J. Alloy. Compd. **552**, 157–165 (2013)
9. A. Sheorana, A. Agarwal, S. Sanghi, V.P. Seth, S.K. Gupta, M. Arora, Phys. B **406**, 4505–4511 (2011)
10. G.P. Singh, D.P. Singh, J. Phys. Chem. Solids **73**, 540–544 (2012)
11. D.M. Martín, M.A. Villegas, J. Gonzalo, J.M. Fernández-Navarro, J. Eur. Ceram. Soc. **29**, 2903–2913 (2009)
12. S.M. Salem, E.K. Abdel-Khalek, E.A. Mohamed, M. Farouk, J. Alloy. Compd. **513**, 35–43 (2012)
13. P. Subbalakshmi, B.V. Raghavaiah, R.B. Rao, N. Veeraiah, Eur. Phys. J. Appl. Phys. **26**, 169 (2004)
14. M. Von Dirke, S. Muller, K. Barner, H. Rager, J Non Cryst. Solids **124**, 265 (1990)
15. S.M. Salem, J. Non Cryst. Solids **358**, 1410–1416 (2012)
16. B.L. Shivachev, T. Petrov, H. Yoneda, R. Titorenkova, B. Mihailova, J. Scripta Mater. **61**, 493–496 (2009)
17. G.P. Singh, S. Kaur, P. Kaur, S. Kumar, D.P. Singh, Phys. B **406**, 1890–1893 (2011)
18. S. Rada, R. Chelcea, M. Rada, A. Bot, N. Aldea, V. Rednic, E. Culea, Electrochim. Acta **109**, 82–88 (2013)
19. B. Sumalatha, I. Omkaram, T.R. Rao, C.L. Raju, J. Mol. Struct. **1006**, 96–103 (2011)
20. M.S. Al-Buriahi, V.P. Singh, A. Alalawi, C. Sriwunkum, B.T. Tonguc, Ceram. Int. **46**, 15464–15472 (2020)
21. A.M. Abdelghany, A.H. Hammad, Spectrochim. Acta A **137**, 39–44 (2015)
22. G.P. Singh, D.P. Singh, Phys. B. **406**, 640–644 (2011)
23. M. Subhadra, P. Kistaiah, Vib. Spectrosc. **62**, 23–27 (2012)
24. M. Farouk· F. Ahmad, A. Samir, Opt. Quantum Electron, 51–292 (2019)
25. L.S. Rao, V.R. Kumar, P. Naresh, P.V. Rao, N. Veeraiah, Mater. Today Proc. **5**, 26290–26297 (2018)
26. N. Laorodphan, P. Pooddee, P. Kidkhunthod, P. Kunthadee, W. Tapalab, R. Puntharod, J. Non Cryst. Solids **453**, 118–124 (2016)
27. J. Singh, D. Singh, S.P. Singh, G.S. Mudahar, K.S. Thind, Mater. Phys. Mech. **19**, 9–15 (2014)
28. R. Iordanova, M. Milanova, L. Aleksandrov, K. Shinozaki, T. Komatsu, J. Non Cryst. Solids **543**, 120132 (2020)
29. V.N. Sigaev, I. Gregora, B. Champagnon, P.D. Sarkisov, J. Non-Cryst, Solids **279**, 136–144 (2001)
30. Y. Gandhi, K.S.V. Sudhakar, M. Nagarjuna, N. Veeraiah, J. Alloy. Compd. **485**, 876–886 (2009)
31. P. Subbalakshmi, N. Veeraiah, J. Phys. Chem. Solids **64**, 1027–1035 (2003)
32. M. Abdel-Baki, F. El-Diasty, J. Solid State Chem. **184**, 2762–2769 (2011)
33. F.H. ElBatal, S.Y. Marzouk, F.M. Ezz-Eldin, J. Non Cryst. Solids **356**, 2750–2759 (2010)
34. B. Bendow, P.K. Banerjee, M.G. Drexhage, O.H. El-Bayoumi, S.S. Mitra, C.T. Moynihan, D. Gavin, G. Fonteneau, J. Lucas, M. Poulain, J. Am. Ceram. Soc. **66**, 64–66 (1983)
35. M.C. Rao, J. Non-Oxide Glasses **5**, 1–8 (2013)
36. D.M. Martin, M.A. Villegas, J. Gonzalo, J.M.F. Navarro, J. Eur. Ceram. Soc. **29**, 2903 (2009)
37. I. Shaltout, Y. Tang, R. Braunstein, E.E. Shaisha, J. Phys. Chem. Solids **57**, 1223 (1996)
38. R.C. Lucacel, I. Ardelean, J. Non Cryst. Solids **353**, 2020 (2007)
39. P. Gunhakoon, T. Thongklom, P. Sopapan, J. Laopaiboon, R. Laopaiboon, O. Jaiboon, Mater. Chem. Phys. **243**, 122587 (2020)
40. D. Boudlich, L. Bih, M.E.H. Archidi, M. Haddad, A. Yacoubi, A. Nadiri, B. Elouadi, J. Am. Ceram. Soc. **85**(3), 623 (2002)
41. M.S. Gaafar, Y.B. Saddeek, L. Abd El-Latif, J. Phys. Chem. Solids **70**, 173–179 (2009)
42. D. Munoz-Martín, M.A. Villegas, J. Gonzalo, J.M. Fernández-Navarro, J. Eur. Ceram. Soc. **29**, 2903–2913 (2009)
43. Y. Gandhi, K.S.V. Sudhakar, M. Nagarjuna, N. Veeraiah, J. Alloys Compd. **485**, 876 (2009)
44. S. Rada, P. Pascuta, M. Culea, V. Maties, M. Rada, M. Barlea, E. Culea, J. Mol. Struct. **924–926**, 89 (2009)
45. A. Edukondalu, Ch. Srinivasu, Syed Rahman, K. Siva Kumar, J. Sci. Eng. Res. **5**(3) (2014)
46. M. Milanova, R. Iordanova, K.L. Kostov, J. Non Cryst. Solids **355**, 379–385 (2009)
47. G. Lakshminarayana, S. Buddhudu, Spectrochim. Acta **63**, 295 (2006)
48. G. Lakshminarayana, S.O. Baki, A. Lira, I.V. Kityk, U. Caldiño, K.M. Kaky, M.A. Mahdi, J. Lumin. **186**, 283–300 (2017)
49. A. Edukondalu, V. Sathe, S. Rahman, K.S. Kumar, Phys. B **438**, 120–126 (2014)
50. L. Aleksandrov, T. Komatsu, K. Shinozaki, T. Honma, Reni Iordanova. J. Non-Cryst. Solids **429**, 171–177 (2015)
51. J.F.V.L. Munhoz, S.H. Santagneli, M. de Oliveira Jr, A.C.M. Rodrigues, H. Eckert, M. Nalin, J. Non Cryst. Solids **505**, 379–389 (2019)
52. J. Yuan, Q. Yang, D.D. Chen, Q. Qian, S.X. Shen, Q.Y. Zhang, Z.H. Jiang, J. Appl. Phys. **111**, 103511 (2012)
53. M.R. Krames, O.B. Shchekin, R.M. Mach, G.O. Mueller, L. Zhou, G. Harbers, M.G. Craford, J. Disp. Technol. **3**, 160–175 (2007)

54. V.O. Sokolov, V.G. Plotnichenko, E.M. Dianov, Neorg. Mater. **43**, 236–256 (2007)
55. R. Agaki, N. Ohtori, N.J. Umessaki, J. Non Cryst. Solids **471**, 293 (2001)
56. M. Milanova, K.L. Kostov, R. Iordanova, L. Aleksandrov, A. Yordanova, T. Mineva, J. Non Cryst. Solids **516**, 35–44 (2019)
57. L. Bih, M. Azrour, B. Manoun, M.P.F. Graça, M.A. Valente, J. Spectrom. **10** (2013)
58. M. Farouk, Optik **140**, 186–196 (2017)
59. Q. Chen, J. Non Cryst. Solids **493**, 20–28 (2018)
60. S. Yusub, T. Narendrudu, S. Suresh, D. Krishna Rao, J. Mol. Struct. **1076**, 136–146 (2014)